Journal of Statistical Physics, Vol. 48, Nos. 5/6, 1987

A Crisis in the Belousov–Zhabotinskii Reaction: Experiment and Simulation

P. Richetti,[1] P. De Kepper,[1] J. C. Roux,[1] and Harry L. Swinney[2]

An abrupt transition that has the character of an *interior crisis* was observed in an experiment on the Belousov–Zhabotinskii reaction as a control parameter was varied (a crisis is a qualitative change in the dynamics of a system observed when an attractor collides with the stable manifold of a fixed point). The interpretation of the observed behavior as a crisis is corroborated by a numerical analysis of a seven-variable model of the reaction. The waveforms, attractors, and maps obtained in the simulation are remarkably similar to those obtained in the laboratory experiment. The simulation indicates that the crisis is a consequence of a multivalued first return map.

KEY WORDS: Nonlinear dynamics; chaos; crisis; Belousov–Zhabotinskii reaction.

1. INTRODUCTION

The term crisis has been coined[1] to describe the sudden qualitative change in dynamical behavior that occurs when a chaotic attractor collides with an unstable coexisting periodic orbit or its stable manifold. For 1D maps the stable manifold is zero-dimensional; then, the crisis occurs by collision with an unstable periodic point. For example, the one-dimensional map

$$x_{n+1} = f(x_n) = rx_n(1 - x_n) \tag{1}$$

can exhibit two different types of crisis as a function of the control parameter r. It is well known that this logistic map yields a subharmonic

[1] Centre de Recherche Paul Pascal, Université de Bordeaux-I, 33405 Talence cedex, France.
[2] Center for Nonlinear Dynamics and Department of Physics, University of Texas, Austin, Texas 78712.

0022-4715/87/0900-0977$05.00/0 © 1987 Plenum Publishing Corporation

bifurcation cascade, which accumulates at $r_\infty = 3.5699456...$.[2,3] On increasing r further, the resulting chaotic attractor undergoes a crisis for $r^* = 4$, where the unstable period-1 orbit collides with the chaotic attractor on its basin boundary; this is called a *boundary* or *exterior* crisis. Beyond r^* the previous chaotic attractor is unstable and for all initial values the system will ultimately diverge to minus infinity. Nevertheless, for $(r - r^*) \ll 1$, if initial conditions are chosen in the previously chaotic region, the system may stay for a relatively long time on the formerly stable chaotic attractor before departing from it. This phenomenon is called transient chaos.

The other type of crisis generated by the map (1) is observed for $r_\infty < r < r^*$, where it is known that periodic windows[4,5] can be observed. These arise from a tangent bifurcation and disappear through a period doubling cascade to produce a multiband chaotic attractor. Beyond a critical value $r = r^0$ each multiband attractor suddenly enlarges to a new, single, broadband attractor in which the previously multiband attractor is immersed. This is an *interior* crisis (or "explosion" of strange attractor[6]): an unstable orbit collides with a coexisting chaotic attractor, resulting in a sudden enlargement in the chaotic attractor. As in the interior crisis, the initial chaotic attractor can be observed as a transient for $r - r^0 \ll 1$.

Similar features are at the origin of these crises. A crisis is observed every time that, on changing a control parameter value, the maximum of a unimodal map exceeds the limit of the invariant interval in which the initial chaotic attractor is located. In both examples one can show that the lifetime probability distribution of transient chaotic behavior decreases exponentially for large time t:

$$P(t) = \langle T \rangle_r^{-1} \exp(-t/\langle T \rangle_r) \tag{2}$$

where $\langle T \rangle_r$ is the mean lifetime at a given value of the control parameter r. Moreover, the mean lifetime scales with the distance to the critical onset point r_c of the crisis

$$\langle T \rangle_r \cong |r - r_c|^{-1/\gamma} \tag{3}$$

where γ is the order of the maximum of the unimodal map.

Crises are ubiquitous in nonlinear systems; they occur whenever a chaotic attractor compete with another attractor, be it a fixed point,[7,8] a limit cycle,[9] or another chaotic attractor.[1] In differential equation systems the associated return maps are not necessarily one-dimensional curves. However, Grebogi *et al.*[10] recently analyzed crises for higher dimensional Poincaré maps. They determined that in this case the critical scaling relation (3) must be modified to take into account the actual dissipation factor of the map.

Very few clear experimental observations of crises have been published. The broadening of a three-band chaotic attractor was thoroughly studied in a diode inductor device[11,12] and the observed behavior fit Eqs. (2) and (3) with a critical exponent γ equal to 2, the generic value for the logistic map Eq. (1). Another crisis was observed in a CO_2 laser with an internal modulation.[13]

In this paper we discuss evidence of an interior crisis resulting from the interaction of two one-band strange attractors in the Belousof–Zhabotinskii (BZ) reaction. The experimental results are presented in Section 2. These are compared with a numerical simulation on a kinetic model of the reaction in Section 3. The striking similarities between the experimental results in Figs. 1, 2, 5, and 7 and the computed behavior in Figs. 3, 4, 6, and 8 provide an understanding of the observed dynamics, as discussed in Section 4. Section 5 is devoted to the analysis of the statistical behavior of the phenomenon, a work only possible numerically because of the long time scales of the experimental dynamics.

2. EXPERIMENTAL RESULTS

The reaction has been performed in a stirred tank reactor described in earlier publications,[14-17] with the following concentrations of chemicals in the mixed feed stream:

$$[BrO_3^-]_0 = 0.1 \text{ M}, \qquad [Ce^{3+}]_0 = 1.7 \times 10^{-3} \text{ M}$$

$$[CH_2(COOH)_2]_0 = 0.25 \text{ M}, \qquad [H_2SO_4]_0 = 0.2 \text{ M}$$

The thermostated temperature was maintained constant at 27°C. The input flow rate k_0 was used as the control parameter. The reaction dynamics was monitored by the electrochemical potential of a bromide-selective electrode.

This composition leads to a domain presenting alternating regions (in the control parameter space) of periodic and chaotic states, which is a behavior often found in the BZ reaction.[14-18] For decreasing flow rate, the following sequence S_1 is observed[16-18]:

$$P_1^0, C_1^{0,1}, P_1^1, C_1^{1,2}, P_1^2, C_1^{2,3}, \ldots, C_r, C_0^n, \ldots, P_0^1 \qquad (S_1)$$

where P and C stand, respectively, for periodic chaotic states and the subscripts and superscripts denote, respectively, the number of large relaxation and small quasisinusoidal oscillations in a periodic pattern; the behavior in the regime C_r that follows the crisis is different—it is discussed below. As suggested by the notation, the chaotic states appear as stochastic mixtures of the adjacent periodic states. The chaotic states are generated from the

adjacent periodic states by subharmonic bifurcation cascades.[19] The resulting sequences are of the form

$$P_1^j \rightarrow C_1^{j,j+1} \rightarrow P_1^{j+1}$$

which have been thoroughly discussed Refs. 14–18. The full sequence S_1, which starts with large-amplitude relaxation oscillations, terminates with small-amplitude, quasisinusoidal oscillations P_0^1.

The C_r chaos has a quite different status. We shall now essentially focus our attention on the $C_0^n \rightarrow C_r$ transition. Figure 1a provides an illustration of a time series of the C_r chaos, while Figs. 1b and 1c, respectively, correspond to time series of the $C_1^{2,3}$ and C_0^n, chaos which are in the immediate vicinity of the previous one. Note that C_r appears as an intermixture of $C_1^{j,j+1}$ and C_0^n types of dynamics.

The relative proportions of $C_1^{2,3}$ and C_0^n regimes strongly depend on the control parameter value. The phenomenon was first thought to be reminiscent of intermittency,[20,21] where a (noisy) laminar phase C_0^n is interrupted from time to time by sudden bursts of chaotic regime $C_1^{j,j+1}$. This interpretation could not be validated, mainly because the C_r dynamics was only observed over a very narrow range of parameter values. Furthermore, it turned out that on improving the accuracy of the pumping device, the observation of C_r-type of dynamics was made still more difficult at the considered chemical constraint values.

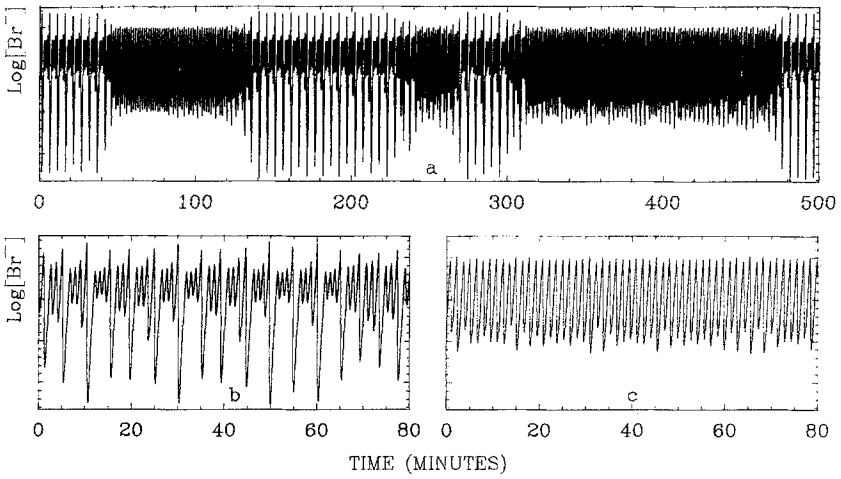

Fig. 1. Bromide ion potential time series illustrating the crisis that occurs as the flow rate is decreased in the experiment on the BZ reaction: (a) the chaotic state C_r, observed after the crisis, (b) the chaotic state $C_1^{2,3}$, which evolves from C_r, (c) the chaotic state C_0^n, observed before the crisis. The corresponding time series obtained in the simulation are shown in Fig. 3.

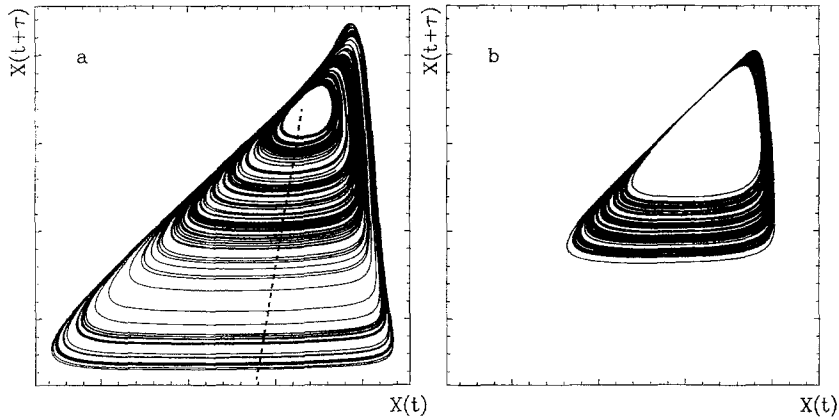

Fig. 2. Phase portraits constructed from the experimental data, illustrating the chaotic attractors (a) after the crisis, C_r, and (b) before the crisis, C_0^n. The corresponding attractors obtained in the simulation are shown in Fig. 4.

However, as we have sketched in the introduction, the evidence that at first argued in favor of intermittency, i.e., the existence of bursts with a mean frequency depending on a control parameter value, can also apply to a crisis. In this case the crisis would be much like the second example given in the introduction. In agreement with this latter interpretation, the transition from C_r to C_0^n is continuous and the final state C_0^n is already embodied in C_r, as is clear from the phase portraits of the two attractors (Fig. 2).

We shall see that our numerical results on a kinetic model of the BZ reaction rather favor this last interpretation.

3. NUMERICAL RESULTS

Our numerical results are based on the following scheme for the kinetics of the BZ reaction[22,23]:

$$BrO_3^- + Br^- + 2H^+ \rightarrow HBrO_2 + HOBr \qquad (k_1 = 2.1 M^{-3} \sec^{-1}) \tag{R1}$$

$$HBrO_2 + Br^- + H^+ \rightarrow 2HOBr \qquad (k_2 = 2 \times 10^9 M^{-2} \sec^{-1}) \tag{R2}$$

$$HOBr + Br^- + H^+ \rightarrow Br_2 + H_2O \qquad (k_3 = 8 \times 10^9 M^{-2} \sec^{-1}) \tag{R3}$$

$$BrO_3^- + HBrO_2 + H^+ \rightleftarrows 2BrO_2^\cdot + H_2O$$

$$(k_4 = 10^4 M^{-2}\,sec^{-1},\ k_{-4} = 111 \times 10^7 M^{-2}\,sec^{-1}) \tag{R4}$$

$$2HBrO_2 \rightarrow HOBr + BrO_3^- + H^+$$

$$(k_5 = 4 \times 10^7 M^{-1}\,sec^{-1}) \tag{R5}$$

$$BrO_2^\cdot + Ce(III) + H^+ \rightarrow Ce(IV) + HBrO_2$$

$$(k_6 = 10^3 M^{-1}\,sec^{-1}) \tag{R6}$$

$$HOBr + MA \rightarrow BrMA + H_2O$$

$$(k_7 = 10^6 M^{-1}\,sec^{-1}) \tag{R7}$$

$$BrMA + Ce(IV) \rightarrow Br^- + R^\cdot + Ce(III) + H^+$$

$$(k_8 = 5 \times 10^3 M^{-1}\,sec^{-1}) \tag{R8}$$

$$R^\cdot + Ce(IV) \rightarrow Ce(III) + P$$

$$(k_9 = 10^8 M^{-1}\,sec^{-1}) \tag{R9}$$

where P is an inert product, and BrMA and R$^\cdot$, respectively, are brominated and oxidized derivatives of malonic acid (MA). From the law of mass action we can generate the following set of differential equations

$$\begin{aligned}
\dot{X}_1 &= -a_1 X_1 - a_2 X_1 X_2 - a_3 X_1 X_3 + k_8 X_5 X_6 + k_0 (X_1^0 - X_1) \\
\dot{X}_2 &= a_1 X_1 - a_2 X_1 X_2 - a_4 X_2 + a_5 X_4^2 - 2k_5 X_2^2 + a_6 X_4 - k_0 X_2 \\
\dot{X}_3 &= a_1 X_1 + 2a_2 X_1 X_2 - a_3 X_1 X_3 + k_5 X_2^2 - a_7 X_3 - k_0 X_3 \\
\dot{X}_4 &= 2a_4 X_2 - 2a_5 X_4^2 - a_6 X_4 - k_0 X_4 \\
\dot{X}_5 &= a_6 X_4 - k_8 X_5 X_6 - k_9 X_5 X_7 - k_0 X_5 \\
\dot{X}_6 &= a_7 X_3 - k_8 X_5 X_6 - k_0 X_6 \\
\dot{X}_7 &= k_8 X_5 X_6 - k_9 X_5 X_7 - k_0 X_7
\end{aligned} \tag{4}$$

where the following assigments are made: $X_1 = [Br^-]$, $X_2 = [HBrO_2]$, $X_3 = [HOBr]$, $X_4 = [BrO_2^\cdot]$, $X_5 = [Ce(IV)]$, $X_6 = [BrMA]$, $X_7 = [R^\cdot]$. The parameters a_i are defined from the rate constants k_i according to

$$a_1 = k_1[BrO_3^-][H^+]^2, \qquad a_2 = k_2[H^+],$$

$$a_3 = k_3[H^+], \qquad a_4 = k_4[BrO_3^-][H^+]$$

$$a_5 = k_{-4}[H_2O], \qquad a_6 = k_6[Ce(III)][H^+], \qquad a_7 = k_7[MA]$$

and $X_1^0 = [Br^-]_0$.

The system (4) has already allowed us to account rather accurately for much complex dynamical behavior observed in the BZ reaction.[22,23] Using the set of constraint values

$$[BrO_3^-]_0 = 5 \times 10^{-2}\text{M}, \quad [MA]_0 = 10^{-3}\text{M}, \quad [Ce(III)]_0 = 1.5 \times 10^{-4}\text{M},$$
$$[H^+]_0 = 1.5\text{M}, \quad [Br^-]_0 = 3.0 \times 10^{-7}\text{M}$$

we have obtained the following chaotic periodic sequence as a function of the flow rate coefficient k_0:

$$P_1^0 \to C_1^{0,1} \to P_1^1 \to C_1^{1,2} \to P_1^2 \to C_1^{2,3} \to P_1^3 \to C_1^{3,4} \to P_1^4$$
$$\uparrow \quad \downarrow$$
$$C_0^n \to 2P_0^1 \to P_0^1$$

The computed succession of states and even the shape of the attractors are strikingly parallel to most of the experimental observations. The main difference from experiments lies in the small hysteresis loop observed in the simulation between P_1^4 and C_0^n. For increasing k_0 a transition is observed between two periodic states (P_1^4 to $2P_0^1$) for $k_0 = k_{01}$; the reverse transition occurs for a flow rate k_{02} ($k_{02} < k_{01}$) from C_0^n to P_1^4. This last transition is a crisis, but no C_r-type chaos is observed in this situation. Nonetheless, the $C_1^{3,4}$ and the C_0^n time series displayed, respectively, in Figs. 3b and 3c compare very well with those presented in Figs. 1b and 1c.

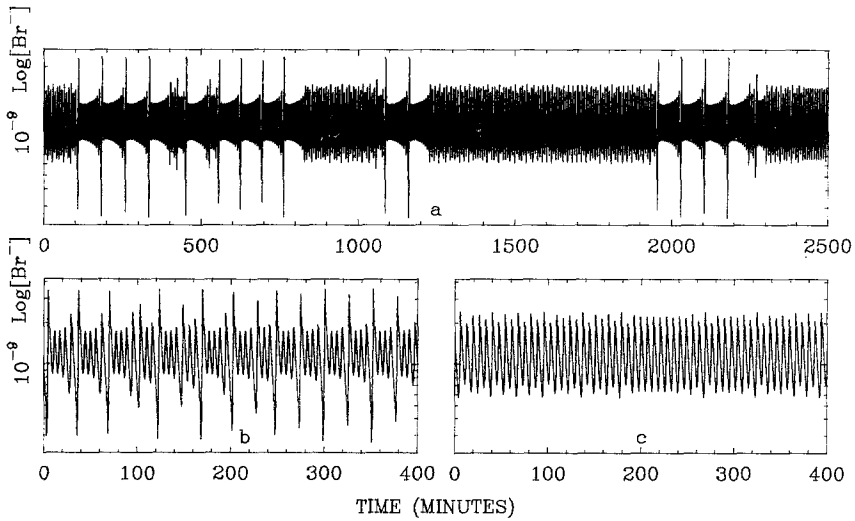

Fig. 3. Time series for log[Br$^-$], obtained in the numerical study of the model: (a) the chaotic state C_r, observed after the crisis, (b) the chaotic state $C_1^{3,4}$, (c) the chaotic state C_0^n, observed before the crisis.

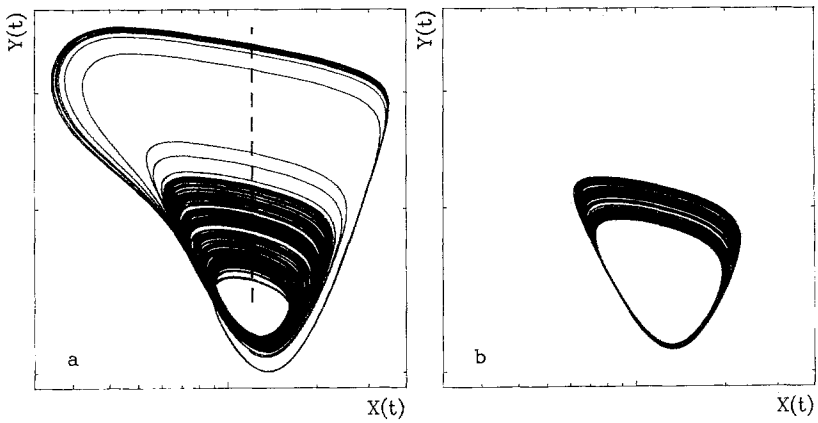

Fig. 4. Phase portraits (with $X = \log[Br^-]$, $Y = \log[Ce(IV)]$), obtained in the numerical simulation, illustrating the chaotic attractors (a) after the crisis, C_r ($k_0 = 3.564160 \times 10^{-3}\,sec^{-1}$) and (b) before the crisis, C_0^n ($k_0 = 3.564248 \times 10^{-3}\,sec^{-1}$).

The transition values k_{01} and k_{02} depend sensitively on the values of the other parameters. If at the upper limit k_{02} the system can be made to undergo a transition from C_0^n to another chaotic state rather than to a periodic state P_1^j, then a C_r type of chaos is generated.

For example, by changing $[Br^-]_0$ to $2.795\ 10^{-7}$ mole/liter, a transition from C_0^n to $C_1^{9,10}$ comes through a C_r-type regime displayed in Fig. 3a. The similarity with the experimental observations (Fig. 1a) is remarkable. As in the experiments, the crisis occurs at the transition between C_0^n and C_r. The attractors obtained in the simulation are shown in Fig. 4, where one can notice that the C_0^n attractor is immersed in the C_r attractor.

The model thus provides us with a very convenient tool to analyze the complex experimental dynamics observed in the BZ reaction. The computed results give more confidence in the experimental observations of chaos (Fig. 1c) which, though not totally free from noise, is not due to stochastic fluctuations in the constraint parameter.

4. POINCARÉ MAPS

Poincaré sections obtained from intersections of the 3D phase space orbits shown in Figs. 2 and 4 with a perpendicular plane going through the dashed lines on these figures are shown Fig. 5 (experiment) and Fig. 6 (simulation). On these maps the points in the upper right corner correspond to the small-amplitude oscillations, which separate the large peak

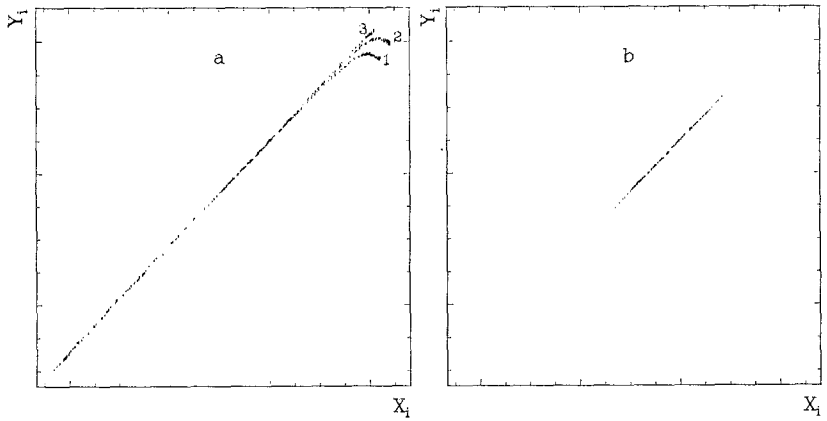

Fig. 5. Poincaré sections for the experimentally obtained chaotic attractors in Fig. 2: (a) for C_r (after the crisis), and (b) for C_0^n (before the crisis). The corresponding Poincaré sections obtained in the simulation are shown in Fig. 6.

oscillations, whereas these large oscillations produce the intersections in the lower left parts of Figs. 5a and 6a. The number of sheets in the upper right part is equal to the number of small-amplitude oscillations. In the computed results only the first two sheets can be clearly distinguished; the others pile up very close to each other and only an enlargment renders them visible. A $C_1^{j,j+1}$ chaotic regime presents very similar topological features, but the multisheeted region corresponding to the small-amplitude oscillations is no longer connected to the zone where the large-amplitude oscillations intersect the Poincaré plane. Thus the main difference between

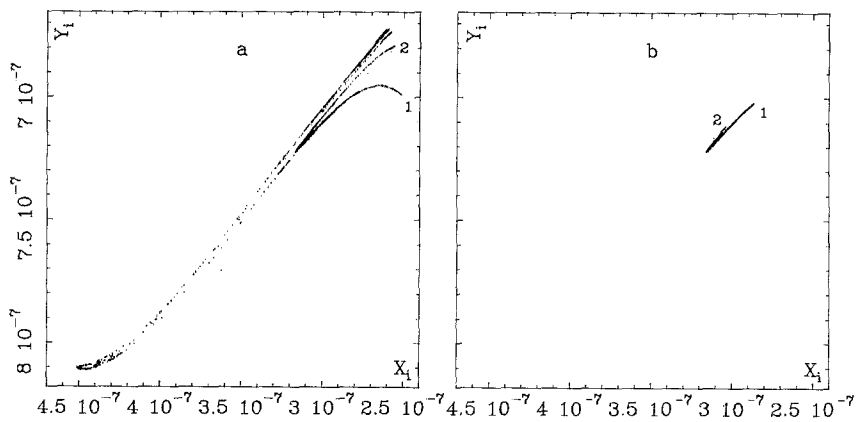

Fig. 6. Poincaré sections for the numerically obtained chaotic attractors in Fig. 4: (a) for C_r (after the crisis), and (b) for C_0^n (before the crisis).

$C_1^{j,j+1}$ and C_r is the existence of a third accumulation region for C_r. This zone corresponds precisely to the location of the Poincaré section of C_0^n, as shown, respectively, in Figs. 5a and 5b and Figs. 6a and 6b plotted on the same scale: C_0^n is contained in C_r. This is even clearer if we take a look at the first return maps displayed in Figs. 7 and 8. We can see from Fig. 8b that the two parts of the C_0^n attractor labeled 1 and 2 have their exact correspondent in the C_r attractor (Fig. 8a).

The numerical and experimental first return maps differ mainly by the amount of noise, which blurs the experimental map. They have the same overall shape, with well-defined multisheeted minima and a broad maximum. This shape is characteristic of all the maps in the periodic chaotic sequence.[19] This type of sequence is relevant to the dynamics close to a homoclinic bifurcation.[24-26]

Let us now focus on the calculated 1D map of C_0^n, just before the crisis (Fig. 9b) and just after (Fig. 9a). In these figures the dashed lines correspond to the calculated "invariant square." The latter is obtained from the first return map for $k_0 = k_0^*$. Before the crisis all points of the map iterate within the "invariant square." After the crisis some points fall outside this square and will escape the attractor on subsequent iteration.

Unfortunately, the experimental noise prevents any similar refined analysis in the bench experiments. However, we can still distinguish on the 1D map of C_r (Fig. 7a) a noisy component corresponding to the contribution of C_0^n. It must also be mentioned that this experimental noise may advance the onset of the crisis before the actual critical parameter

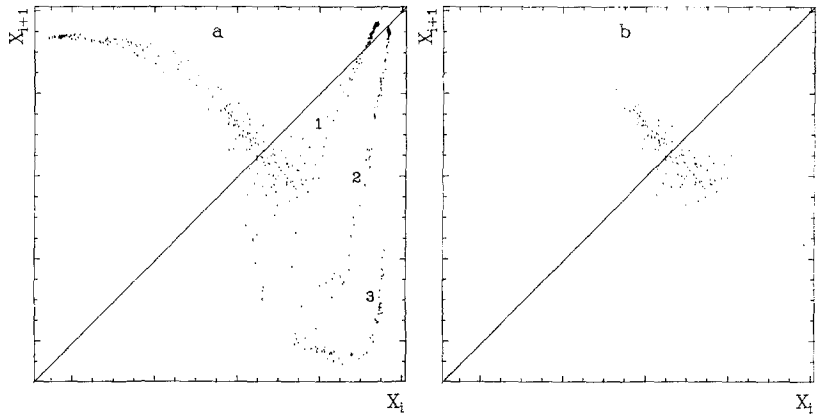

Fig. 7. First return maps obtained from the Poincaré sections (in Fig. 5) for the experimental data: (a) for C_r (after the crisis), and (b) for C_0^n (before the crisis). The corresponding first return maps obtained in the simulation are shown in Fig. 6.

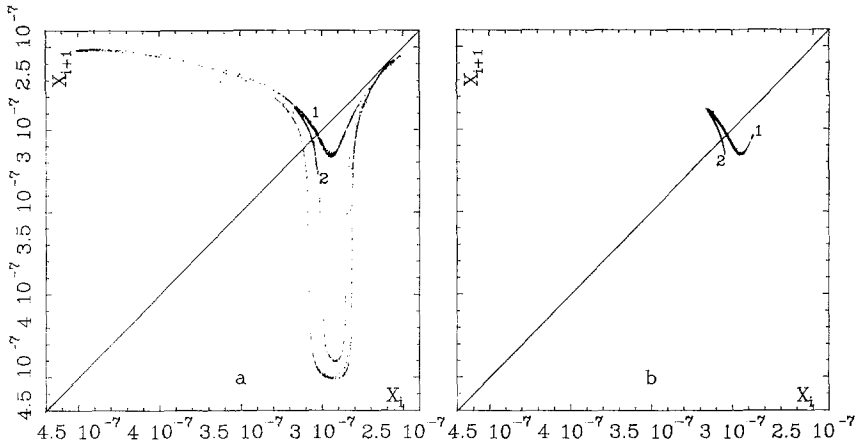

Fig. 8. First return maps computed for the Poincaré sections (in Fig. 6) from the numerical simulation: (a) for C_r (after the crisis), and (b) for C_0^n (before the crisis). An enlargement of the central portion of these maps is shown in Fig. 9.

value is attained. This may explain the effects of changing the accuracy of the pumping devices.

In order to get a better understanding of the evolution from C_1^n to C_r we present an overview of the evolution of the 1D maps of the chaotic states from $C_1^{0,1}$ to $C_1^{n,n+1}$ gained from the study of the model. As explained previously, each chaotic state in this sequence differs from the preceding one by the addition of one extra small-amplitude oscillation; this translates

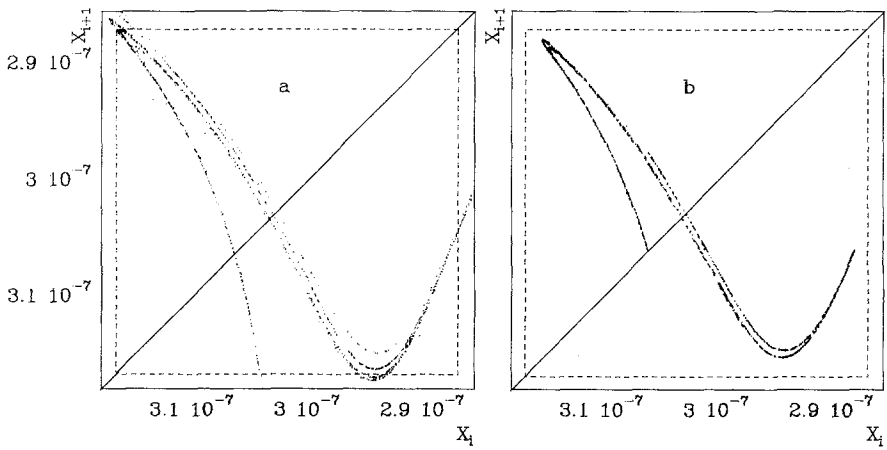

Fig. 9. Enlargement of the central portion of the multisheeted first return maps in Fig. 8, obtained in the numerical simulation: (a) for C_r (just after the crisis), and (b) for C_0^n (just before the crisis). The dashed box is the "invariant square."

on the Poincaré map into the emergence of a new sheet. On the 1D map the addition of a new sheet comes with a wider separation of the sheets (in fact, each sheet has a Cantor set-like structure). This accumulation of sheets terminates when the last sheet added is part of the C_0^n attractor.

5. CRITICAL BEHAVIOR

In the neighborhood of a crisis the dynamics should exhibit universal properties described by a characteristic exponent, but few studies in physical systems[11,12] have examined this behavior. In our work the critical behavior could be analyzed from the integration of (4), but a detailed experimental study was not possible because of the critical slowing down near transition. Even the calculations are very lengthy and costly because of the high dimensionality of the system (seven independent variables) and the stiffness of the resulting dynamics.

The critical value of the control parameter was determined by trial and error and found to be $k_0^* = 3.5640246 \times 10^{-3}\ \text{sec}^{-1}$. Figure 10a presents the distribution function of the transient chaos of the attractor C_0^n for $k_0 = 3.5640160 \times 10^{-3}\ \text{sec}^{-1}$. This distribution function was built from 10^5 chaotic transients. We can see that the exponential decay (2) is verified, at least for large N. Figure 10b shows the variation of $\langle N \rangle$ with the distance to k_0^*. Each mean value was derived from at least 500 transient chaotic states. From the log–log plot we find a characteristic exponent $\gamma = 1.54$ for $|k_0 - k_0^*|/k_0^* < 0.15$.

We recall that $\gamma = 2$ is obtained only in the limit of infinite dissipation. In our system, due to finite dissipation rate and to the associated Cantor set structure of the return map, a deviation from this value could be expected.[10] Our estimate of the exponent was made over less than two

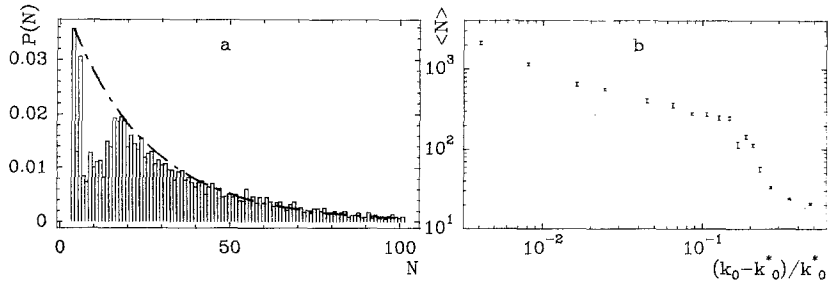

Fig. 10. Statistics of the transient chaos obtained in the numerical simulation. (a) The number of surviving C_r-type orbits after N orbits for a C_0^n attractor; $k_0 = 3.564160 \times 10^{-3}\ \text{sec}^{-1}$. Fit calculated from Eq. (2) (- - -). (b) The computed dependence of the average lifetime of the transient C_r-type chaos in the C_0^n regime as a function of the distance to the critical point k_0^*.

orders of magnitude range in control parameter because computation time becomes prohibitively long in the vicinity of the critical point.

Nevertheless, the results corroborate our analysis (Section 4) of the phenomenon. As shown in Fig. 9a, the crisis occurs as soon as at least one fold extends beyond the "invariant square." Furthermore, note that the dependence of $\langle N \rangle$ changes dramatically when the relative distance to the critical point becomes greater than 10%; this is apparently due to the contribution of a new fold coming through the "invariant square."

6. CONCLUSIONS

The remarkable similarity of the results from numerical simulations (shown in Figs. 3, 4, 6, and 8) and the corresponding experimental results (shown in Figs. 1, 2, 5, and 7) provides strong support for the interpretation of the observed sudden change in the dynamics as a crisis, even though the noise in the data preclude a quantitative comparison with theory.

Similar dynamics should be observed in any system exhibiting a multivalued first return map with a single extremum. For example, compare our Figs. 1 and 9 with Figs. 4 and 5 in Ref. 12, obtained in a study of a laser system.

ACKNOWLEDGMENTS

We thank K. Coffman for valuable experimental observations. The laboratory experiments were conducted at the University of Texas during visits of P. R., P. De K., and J. C. R. to the Texas laboratory. The research in Texas was supported by the Department of Energy Office of Basic Energy Sciences.

REFERENCES

1. C. Grebogi, E. Ott, and J. A. Yorke, *Physica (Amsterdam)* **7D**:181 (1983); *Phys. Rev. Lett.* **48**:1507 (1982).
2. M. J. Feigenbaum, *J. Stat. Phys.* **19**:25 (1978); **21**:669 (1979).
3. P. Coullet and C. Tresser, *J. Phys. (Paris)* **39**:C-5 (1978).
4. N. Metropolis, M. L. Stein, and P. R. Stein, *J. Combinatorial Theory Ser.* A **15**:25 (1973).
5. P. Collet and J. P. Eckmann, *Iterated Maps of the Interval as Dynamical Systems* (Birkhauser, Boston, 1980).
6. Y. Ueda, *Ann. N. Y. Acad. Sci.* **357**:422 (1980).
7. J. A. Yorke and E. D. Yorke, *J. Stat. Phys.* **21**:263 (1979).
8. P. Richetti, F. Argoul, and A. Arneodo, *Phys. Rev. A* **34**:726 (1986).
9. B. A. Huberman and J. P. Crutchfield, *Phys. Rev. Lett.* **43**:1743 (1979).

10. C. Grebogi, E. Ott, and J. A. Yorke, *Phys. Rev. Lett.* **57**:1284 (1986).
11. R. W. Rollins and E. R. Hunt, *Phys. Rev. A* **29**:3327 (1984).
12. R. C. Hilborn, *Phys. Rev. A* **31**:378 (1985).
13. D. Dangoisse, P. Glorieux, and D. Hennequin, *Phys. Rev. Lett.* **57**:2657 (1986).
14. J. L. Hudson, M. Hart, and D. Marinko, *J. Chem. Phys.* **71**:1601 (1979).
15. J. C. Roux, A. Rossi, S. Bachelart, and C. Vidal, *Physica* **2D**:395 (1981).
16. J. S. Turner, J. C. Roux, W. D. McCormick, and H. L. Swinney, *Phys. Lett.* **85A**:9 (1981).
17. F. Argoul, A. Arneodo, P. Richetti, and J. C. Roux, *J. Chem. Phys.* **86**:3325 (1987).
18. H. L. Swinney and J. C. Roux, in *Non-Equilibrium Dynamics in Chemical Systems*, C. Vidal and A. Pacault, eds. (Springer-Verlag, 1984), p. 124, and references therein.
19. K. Coffman, W. D. McCormick, H. L. Swinney, and J. C. Roux, in *Non-Equilibrium Dynamics in Chemical Systems*, C. Vidal and A. Pacault, eds. (Springer-Verlag, 1984), p. 231.
20. H. L. Swinney, J. Gollub, and N. Abraham, *Physica* **11D**:252 (1984).
21. P. DeKepper, J. C. Roux, and H. L. Swinney, unpublished results.
22. P. Richetti and A. Arneodo, *Phys. Lett.* **109A**:359 (1985).
23. P. Richetti, J. C. Roux, F. Argoul, and A. Arneodo, *J. Chem. Phys.* **86**:3339 (1987).
24. P. Gaspard, R. Kapral, and G. Nicolis, *J. Stat. Phys.* **35**:697 (1984).
25. F. Argoul, A. Arneodo, and P. Richetti, *Phys. Lett.* **120A**:269 (1987).
26. F. Argoul, A. Arneodo, and P. Richetti, in preparation.